IEEE Access
Multidisciplinary | Rapid Review | Open Access Journal

Received July 17, 2019, accepted August 5, 2019, date of publication August 15, 2019, date of current version August 29, 2019.

Digital Object Identifier 10.1109/ACCESS.2019.2935620

Angle-of-Arrival Estimation in Formation Flying Satellites: Concept and Demonstration

ALEXANDRU MIHAI CRISAN, ALEXANDRU MARTIAN, REMUS CACOVEANU, AND DANIELA COLTUC

CEOSpaceTech Research Centre for Spatial Information, University Politehnica of Bucharest, 060042 Bucharest, Romania

Corresponding author: Daniela Coltuc (daniela.coltuc@upb.ro)

This work was supported by the Romanian National Authority for Scientific Research under the Programme Space Technology and Advanced Research (STAR) under Grant 363—HybridNAVCOM.

ABSTRACT One of the challenges of future space missions is the deployment of instruments distributed across multiple satellites that fly in an autonomous formation. This type of mission requires that the spacecraft communicate using inter-satellite links (ISL) and collaborate to fulfil the role of a large-scale, complex scientific instrument. In this context, precise information regarding the relative positioning of the satellites in terms of distance and orientation is essential. In radio frequency (RF) based techniques, obtaining the relative orientation between the satellites starts with estimating the angle-of-arrival (AoA) of the radio signal. This paper proposes an AoA estimation technique that can be used in Orthogonal Frequency-Division Multiplexing (OFDM) communications. Our approach consists in obtaining the AoA using the ISL, specifically the preamble whose primary roles are data link synchronization and channel estimation. Our technique allows a more accurate measurement of the AoA due to an improved ambiguity resolution of phase measurements. We give theoretical results regarding the accuracy of the AoA estimator and we validate them by tests on a real-time functioning testbed consisting in multiple National Instruments Universal Software Radio Peripheral platforms. We show that the carrier frequency offset introduces only a negligible bias in the AoA estimation and we discuss the effect of multipath propagation.

INDEX TERMS Angle-of-arrival, inter-satellite link, orthogonal frequency division multiplexing, universal software radio peripheral.

I. INTRODUCTION

Many potential future science missions, such as interferometer missions and optical or ultraviolet deep space imagers would call for instrument apertures or baselines beyond the scope of deployable structures. The practical approach for providing the measurement capability required by such missions is precision formation flying (PFF) of distributed instruments. PFF refers to multiple satellites that continually communicate and cooperate to achieve the goal of a single, larger and more complex structure.

Knowledge of the relative position is crucial to synthesize structures for large instruments. Direct optical and radio frequency sensing (RF) of inter-satellite range and orientation are essential, especially for missions that cannot fully utilize global positioning system (GPS) capabilities. Space-qualified, high-precision metrology systems with a large dynamic range and the ability to simultaneously track multiple neighboring spacecraft are required.

Although common satellite applications include land mobile satellite systems [1], satellite terrestrial relay networks [2] or fixed satellite service [3], our paper is focused on *space-to-space* satellite applications. Recently several scientific missions for autonomous formation flying satellites have been developed. For instance, PRISMA, which was launched in 2010, was designed to demonstrate formation flying and rendezvous technologies [4]. Another example is PROBA-3, scheduled to launch in 2020, whose primary mission is to demonstrate formation flying technologies of multiple spacecraft. The scientific payload of PROBA-3 consists in a large-length distributed coronagraph used to study the Sun's corona [5].

In formation flying satellites, when GPS data is not available, the relative positioning is usually estimated using

The associate editor coordinating the review of this article and approving it for publication was Nan Wu.

dedicated hardware. Examples of optical sensors include the Vision Based Sensor (VBS) in PRISMA [6] or the Coarse Lateral Sensor (CLS) and the Fine Lateral and Longitudinal Sensor (FLLS) in PROBA-3 [5]. In PRISMA, the VBS can identify the TARGET satellite at distances up to 500 km and can track it down to 10 m during approach maneuvers [7]. The accuracy of CLS is 3.5 arcsec in a field-of-view of ± 5 arcdeg [8]. FLLS is expected to provide lateral and longitudinal accuracies of 21 and 30 μm, respectively [9].

The Formation Flying Radio Frequency (FFRF) sensor deployed in PRISMA falls under the category of RF based metrology systems. FFRF achieved accuracies of 1 cm on distance and 1° on Line-of-Sight (LoS) for low signal elevations [10]. In the case of higher elevations, the performances degraded because of high multipath errors. The LoS is computed based on an antenna triplet: the path differences between the receiver antennas are measured and then the LoS components are calculated [6]. In PRISMA, two inter-satellite links (ISL) are implemented: the main link is in the UHF band and is used to communicate position and status information; the second link is implemented in the FFRF in S-band and is used to transfer metrology measurements. For PROBA-3, the accuracy of the GPS system onboard is specified at 7.5 cm at orbit perigee [11]. The GAMALINK system that is used to implement the ISL contains a redundant GPS system with positioning precision of 5 m.

All these solutions use dedicated hardware, which means an increased budget in terms of energy consumption, mass and satellite volume. A rationale solution from this point of view is to control the relative position by using the existing RF ISL. Such solution implies few supplementary hardware and moderate computational effort.

In RF-based techniques, the estimation of relative orientation starts with calculating the angle-of-arrival (AoA) of the ISL. In formation flying missions single-carrier communication is commonly employed [4]. This paper investigates a method for measuring the AoA in the case of an ISL that employs Orthogonal Frequency-Division Multiplexing (OFDM). In wireless communications, the main advantages of OFDM are the high spectral efficiency, robustness against narrow-band effects, inter-symbol interference and fading and simple channel equalization. One of the drawbacks of OFDM could be high peak-to-average power ratio, but this effect can be compensated by techniques such as signal predistortion [12].

In our approach the preamble that serves to synchronize the ISL in time and frequency and to estimate the channel is also used to obtain the AoA. More precisely, the AoA is estimated by measuring the correlation of preambles received by a couple of antennas. Based on this idea, we derive an analytical expression for the AoA and analyze the impact of several factors on the precision of the AoA estimate. In order of presentation these factors are: the sampling frequency, the receiver noise, the FFT size, the Carrier Frequency Offset (CFO) and multipath propagation. Compared to PRISMA or PROBA-3, our approach is different in the following aspects: a single ISL is jointly used for data communication and AoA estimation, no secondary, dedicated link is needed and no optical systems are employed. Thus, our solution reduces the hardware that needs to be deployed on the satellite platform.

The idea of using the OFDM preamble for AoA measurement was published in our previous work [13]. This paper extends the work in [13] in the following aspects:

1) We improve the precision of AoA estimate by resolving in a different way the ambiguity in measuring the correlation phase. By our approach, the precision of AoA measurement is improved by an order of magnitude.
2) We show that the CFO introduces a bias in AoA estimation and we derive an expression for this bias that linearly depends on the CFO and the sampling period. We demonstrate by simulations and real-time measurements that the bias is negligible for common residual CFO values.
3) We implemented an ISL in real-time using National Instruments Universal Software Radio Peripheral USRP) platforms to test and validate our theoretical results. The test bed allows to simulate AoAs in the range $[-30°, 30°]$ and channels with various SNRs.

The rest of the paper is organized as follows: Section II presents related work regarding RF-based AoA estimation techniques in both ground-based and GPS systems. Section III describes the system model, special subsections being devoted to path difference measurement by correlation method, *wide-lane* technique and Half-Cycle Rounding (HCR), which is our approach for phase ambiguity resolution. Occasionally, simulation results are included to support the theoretical assertions. Section IV discusses the errors introduced in AoA estimation by CFO and multipath propagation. Section V describes the USRP testbed and the results obtained with real-time measurements. Finally, Section VI concludes the paper.

II. RELATED WORK

Most AoA estimation algorithms are based on antenna arrays. The algorithms are implemented using conventional, subspace, maximum likelihood (ML) or integrated techniques.

Conventional methods are based on beamforming, require a large number of elements to achieve high resolution and do not exploit the statistical properties of the useful signals or the noise [14]. One of these techniques is the Delay-and-Sum method, also known as classic beamforming [15]. It is one of the simplest AoA estimation algorithms and is based on performing the weighted sum of the signals received by the antennas. This method has many disadvantages, such as poor resolution, which could be increased by adding more sensors (which ultimately leads to more receivers and storage capacity for the calibration data). Another conventional method is Capon's Minimum Variance [16], which aims to increase the resolution of the Delay-and-Sum method. Capon's method estimates the data covariance matrix and minimizes the output power such that the gain in the desired direction is unitary. This implies steering the beam electronically towards the

correct direction while attenuating other signals that impinge on the sensor array from other directions [17]. Capon's technique is able to detect signals arriving from closely spaced sources compared to the first method but fails if multiple correlated signals are present. In [18] an extension of Capon's method that takes into account the uncertainty in the sensor array manifold is provided.

Subspace based methods aim to improve the resolution of conventional techniques and are based on eigen decomposition of the covariance matrix of the received signals. The most popular technique from this category is Multiple Signal Classification (MUSIC) [19], which is a signal parameter estimation algorithm that provides information about the number of incoming signals, their AoAs, noise power. Various modifications of the MUSIC algorithm have been proposed to increase its resolution and decrease the computational complexity. The authors in [20] propose an improved version of MUSIC that can consistently separate closely spaced sources. Root-MUSIC [21] is based on polynomial rooting, but can be applied only with uniform spaced linear arrays. Cyclic MUSIC [22] exploits the spectral coherence properties of the incoming signals. In [23] it is shown that Root-MUSIC outperforms other techniques in the case of two closely spaced users. Most implementations of MUSIC and Capon in the literature use antenna elements spaced at $\lambda/2$ in order to avoid phase ambiguities. In the case of formation flying satellites, the accuracy demands could require longer baselines.

Estimation of Signal Parameters via Rotational Invariance Technique (ESPRIT) is another subspace-based method which reduces the computational and storage requirements of MUSIC. ESPRIT does not involve extensive search throughout all possible steering vectors [24]. However, it requires that the sensor array can be decomposed into two identical subarrays whose elements are displaced by a fixed translational distance [25]. In [24] it is shown that MUSIC outperforms ROOT MUSIC and ESPRIT in Space Division Multiple Access systems.

ML techniques [26] outperform subspace methods, especially in low SNR conditions, but are very computationally expensive because they require solving nonlinear equations and are rarely implemented in real-time scenarios. In [27] a lower complexity, iterative ML technique for GPS AoA estimation that outperforms Capon and MUSIC in low SNR conditions is proposed. Another iterative ML technique for GPS AoA using a uniform linear array sensor configuration that provides accurate estimations at SNR values under -20 dB is proposed in [28].

The integrated techniques estimate the AoA of the LoS and multipath components of a signal from their spatial signature [29]. Similarly to subspace methods, the spatial covariance matrix is computed, followed by eigen decomposition.

Other RF techniques, such as [30], [31] and [32], implement Kalman filtering to improve the accuracy of AoA estimation.

Several Global Navigation Satellite System (GNSS) based methods have also been developed. For example, two methods for low Earth orbit satellite attitude determination using GPS are proposed in [33]: one is based on carrier phase measurements and the other exploits the received signal strength considering the GPS antenna radiation pattern. The accuracy of the second technique was very low (up to 10°). The authors in [34] propose a GNSS based attitude determination system for nanosatellites using a single antenna and GNSS-derived accelerations whose accuracy is 0.6°.

III. SYSTEM MODEL

We consider a formation composed of two spacecraft: one is the master and performs the metrology tasks, and the second satellite is the slave and acts as a positioning reference. The measurement of AoA requires one transmission antenna at the slave satellite and two receiver antennas at the master satellite. If the two satellites are not aligned, the wavefront emitted by the transmitter antenna Tx travels different distances, d_1 and d_2, to the receiver antennas Rx1 and Rx2 (Fig. 1). The estimation of the AoA denoted by α in Fig. 1 is based on the measurement of the path difference $d_2 - d_1$. For the purpose of this model, the distance y between satellites is considered to be the distance from the Tx antenna of the slave to the center of the Rx antenna baseline at the master, instead of the distance between the center of masses of the satellites. Fig. 1 is a representation of the flight formation geometry used to derive the mathematical relation between α and $d_2 - d_1$. The segments a and b are functions of α:

$$a = r \cdot cos(\alpha) \quad b = r \cdot sin(\alpha) \tag{1}$$

The distances from the Tx antenna to the receiver antennas Rx1 and Rx2 are:

$$d_1 = \sqrt{(y-b)^2 + a^2} \quad d_2 = \sqrt{(y+b)^2 + a^2} \tag{2}$$

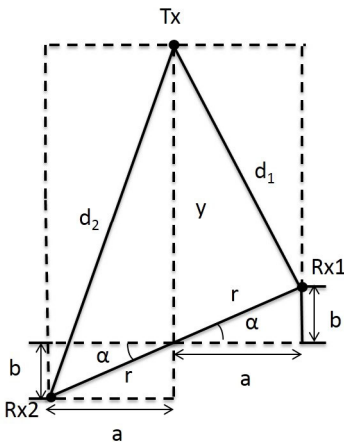

FIGURE 1. Flight formation geometry for estimating the AoA in one plane. Tx is the transmitter antenna located on the slave satellite, Rx1 and Rx2 are the receiver antennas located on the master satellite forming one of the rows of the triplet, and 2r is the antenna baseline length.

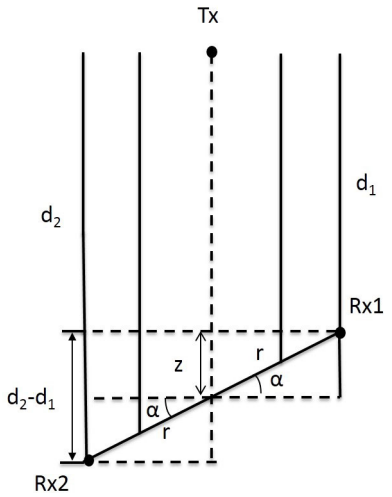

FIGURE 2. Flight formation geometry for a planar wavefront.

Substituting a and b and solving by respect to the difference $d_2 - d_1$, we obtain the following equation for α:

$$\alpha = arcsin\frac{(d_2 - d_1)\sqrt{4r^2 + 4y^2 - (d_2 - d_1)^2}}{4ry} \tag{3}$$

This equation shows that the angle α can be obtained from the path difference $d_2 - d_1$, when the distance y is known. The path difference is estimated by measuring the phase difference between the signals received on Rx1 and Rx2 (the method is detailed in Section III-A). The following shows that the knowledge of y is not necessary if the inter-satellite distance is long enough.

As known, at long distances the spherical wavefront can be approximated by a planar wavefront (Fig. 2). This approximation allows a simplified calculation of α. In Fig. 2, if the segment z is written as:

$$z = r \cdot sin(\alpha) \tag{4}$$

then the two distances are:

$$d_1 = y - z \quad d_2 = y + z \tag{5}$$

and the path difference becomes:

$$d_2 - d_1 = 2z \tag{6}$$

By substituting (4) in (6), the following simplified equation is obtained for α:

$$\alpha = arcsin\frac{d_2 - d_1}{2r} \tag{7}$$

This equation is an approximation of (3). It can be derived directly from (3) by considering y much larger than $d_2 - d_1$ and r, in which case the only relevant term under the square root remains $4y^2$ that cancels the denominator. The major advantage of using this approximation is that the inter-satellite distance y is no longer necessary for the estimation of α that now relies only on the difference $d_2 - d_1$. Thus, by using the planar wavefront approximation, the AoA

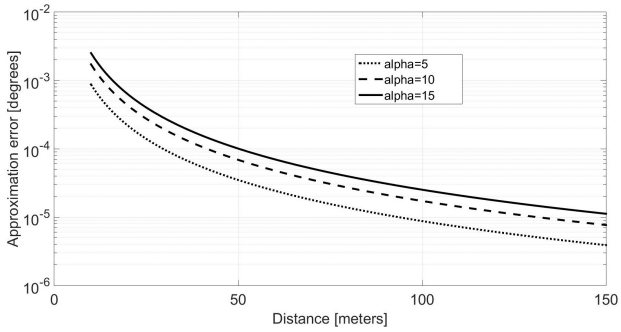

FIGURE 3. Error in the approximation of α with (7) vs. distance (results obtained by MATLAB simulations).

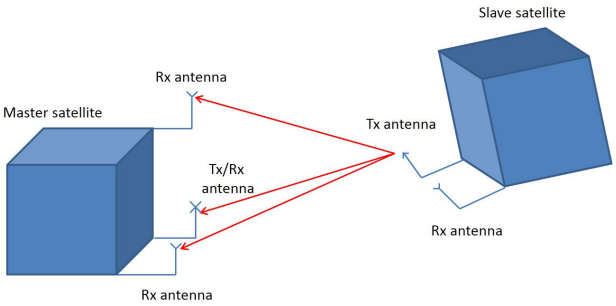

FIGURE 4. Representation of the antenna triplet. The master satellite estimates the relative orientation using the signals received by the three antennas.

calculation is simplified and decoupled from ranging. Fig. 3 shows the approximation error when α is calculated with (7). The error depends on both α and the distance y. Considering a conservative antenna separation of 37.5 cm, imposed by the size of the satellite face (which are in the range of 40 to 130 cm) and an $\alpha = 15°$, at the minimum inter-satellite distance $y = 25$ m where autonomous flying is employed in PROBA-3 and where the accuracy must be highest, using (7) to calculate the AoA introduces an error of only 0.0026%, meaning about 0.0004°. For the same α (least favourable case considered), at distances greater than 100 m, the approximation error drops under 0.0002°.

The relative orientation is a more complex task that demands the measurement of AoA in different planes. A solution can be the triplet method, which requires two orthogonal antenna rows, each row consisting in two receiver antennas (Fig. 4) [35]. One row is used to estimate the pitch angle while the other estimates the yaw angle.

A. ESTIMATION OF PATH DIFFERENCE BY CORRELATION MEASUREMENT

The path difference $d_2 - d_1$ can be obtained by measuring the correlation between the signals received by the two antennas. Next we show how this difference is estimated in the case of an OFDM transmission with a preamble composed of a unique symbol.

An OFDM symbol has N subcarriers $X[k]$, equally spaced in frequency. With an intercarrier spacing of F_s/N, the subcarrier frequencies can be written as

$$F_k = F_c + k\frac{F_s}{N} \tag{8}$$

where F_c is the central frequency of the channel and F_s is the sampling frequency.

On an ideal channel – without noise or multipath effects – after traveling a distance d, each subcarrier is subject to a phase shift described by the phasor $e^{-jd\beta_k}$, where β_k is equal to $2\pi F_k/c$. Therefore, the subcarriers of the OFDM symbol received by the two antennas will be:

$$\begin{aligned} Y_1[k] &= X[k]e^{-j2\pi\frac{d_1}{c}(F_c+k\frac{F_s}{N})} \\ Y_2[k] &= X[k]e^{-j2\pi\frac{d_2}{c}(F_c+k\frac{F_s}{N})} \end{aligned} \tag{9}$$

In time domain, the corresponding signals are $y_1(t)$ and $y_2(t)$.

The difference $d_2 - d_1$ is estimated from the correlation of y_1 and y_2:

$$R(\tau) = \int_0^{NT-1} y_1(t+\tau)y_2^*(t)dt \tag{10}$$

where $T = 1/F_s$. For practical reasons, the correlation is calculated on a limited time support equal to the length of OFDM symbol. At $\tau = 0$, the two received symbols are perfectly superposed. This produces a maximum at the level of the correlation modulus and, the following spectrum in the frequency domain (according to the cross-correlation theorem):

$$\mathcal{F}\{R(\tau)\} = Y_1[k]Y_2^*[k] = |X|^2\, e^{j2\pi\frac{d_2-d_1}{c}F_c} e^{j2\pi\frac{d_2-d_1}{c}k\frac{F_s}{N}} \tag{11}$$

where $|X|$ is the absolute value of $X[k]$, which is constant for the OFDM preamble symbol. By inverse Fourier Transform one obtains the following expression of $R(\tau)$:

$$\begin{aligned} R(\tau) &= |X|^2 e^{j2\pi(d_2-d_1)\frac{F_c}{c}} \sum_{k=-\frac{N}{2}}^{k=\frac{N}{2}-1} e^{j2\pi\frac{d_2-d_1}{c}k\frac{F_s}{N}} e^{j2\pi\frac{k}{NT}\tau} \\ &= |X|^2 e^{j2\pi(d_2-d_1)\frac{F_c}{c}} \sum_{k=-\frac{N}{2}}^{k=\frac{N}{2}-1} e^{j2\pi\frac{k}{N}[\frac{d_2-d_1}{c}F_s+\frac{\tau}{T}]} \end{aligned} \tag{12}$$

The sum in (12) is the inverse Fourier Transform of a constant, meaning a shifted Dirac in time domain. It is evident that the phase of correlation is given only by the exponential in front of the sum:

$$\phi_{max} = 2\pi(d_2 - d_1)\frac{F_c}{c} \tag{13}$$

The subscript *max* stresses the fact that this result is valid only for $\tau = 0$ i.e., when the correlation modulus is maximum. This obliges the detection of the maximum of the correlation and the measurement of the phase exactly at that moment in order to be able to use ϕ_{max} for the estimation of path difference:

$$d_2 - d_1 = \frac{c}{2\pi F_c}\phi_{max} = \frac{\lambda_c}{2\pi}\phi_{max} \tag{14}$$

By including this result in (7) we obtain the following approximation for α:

$$\alpha \approx arcsin\left(\frac{\lambda_c}{4\pi r}\phi_{max}\right) \tag{15}$$

At the master, the cross-correlation is calculated after the synchronous sampling of y_1 and y_2 meaning that only samples of the cross-correlation are available. With high probability the maximum of the cross-correlation falls between two sampling moments, meaning that the detected maximum is not the actual peak of the correlation but a point in its vicinity. In this case, since the condition of perfect superposing is no longer satisfied, the sum in (12) will have in most cases a non-zero phase that introduces an error in the path difference estimation. This error depends on the content of the OFDM signal and on the sampling frequency. Considering $F_s = 7.68$ MHz and $F_c = 1.2$ GHz, an example of the phase variation of the sum in (12) around the correlation maximum when $\alpha = 10°$ is shown in Fig. 5. The phase variation has been obtained by oversampling y_1 and y_2 with a factor of 100. The axis of abscissas corresponds to the domain $[-T/2, T/2]$. It can be seen that the phase is 0 in the origin. The variation of the phase around the maximum depends on how the subcarriers of the training symbol are modulated. We simulated the phase measurement for 10000 different pseudo-random symbols, in the most unfavourable case ($\tau = T/2$). The histogram of the errors induced in the estimation of α is shown in Fig. 6. The standard deviation of the distribution is 0.0045°. The variation of the sampling frequency did not significantly change the error distribution. All of these show that the sampling introduces only a negligible error in the AoA estimation.

B. PHASE AMBIGUITY RESOLUTION BY

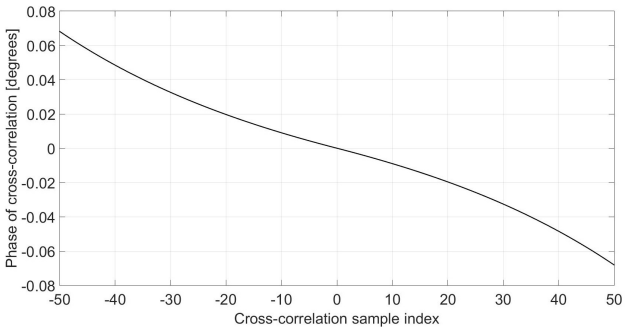

FIGURE 5. Phase variation of the sum in (12) around the cross-correlation maximum at $\alpha = 10°$ and a particular pseudo-random modulation sequence. The received signals are oversampled with a factor of 100 (results obtained by MATLAB simulations).

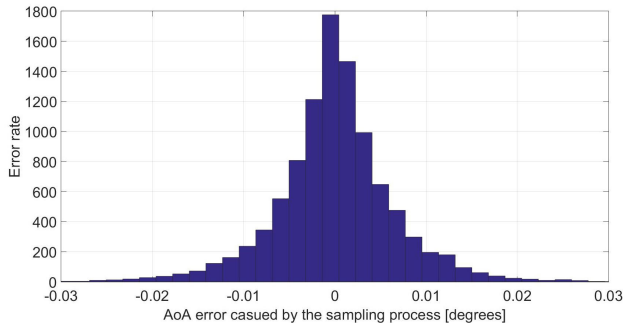

FIGURE 6. Histogram of the errors in the estimation of α caused by the sampling process, for $\tau = T/2$. The received signals are oversampled with a factor of 100 (results obtained by MATLAB simulations).

WIDE-LANE TECHNIQUE

The path difference can be estimated correctly from ϕ_{max} only if the half-wavelength condition is satisfied [36]:

$$2r \leq \lambda_c/2 \tag{16}$$

Because of physical dimensions of the satellite, the distance between the two receiver antennas sometimes does not satisfy this condition. In these cases, the measured phase is only the fractional part of the actual phase. The unsensed part of the phase is an unknown number of π's. A solution to resolve this ambiguity is to use two OFDM signals transmitted on channels with central frequencies F_{c1} and F_{c2}, respectively. The second channel can also be used for frequency diversity or to increase the data rate of the ISL. With this configuration instead of considering the phase ϕ_{max} of a single channel, one measures the difference of phases on the two channels [37]:

$$\phi_{max,wl} = \phi_{max,F_{c2}} - \phi_{max,F_{c1}} \tag{17}$$

This is equivalent to using a single central frequency $F_{wl} = F_{c1} - F_{c2}$. The subscript wl comes from the name of the technique known as *wide-lane*. By choosing F_{c1} and F_{c2} sufficiently close, the wavelength λ_{wl} can be tuned such to satisfy the half-wavelength condition [37]:

$$\lambda_{wl} = \frac{c}{F_{wl}} = \frac{c}{F_{c2} - F_{c1}} \geq 4r \tag{18}$$

The downside of the *wide-lane* technique is the precision. The measurement of $\phi_{max,F_{c1}}$ and $\phi_{max,F_{c2}}$ is corrupted by the receiver noise, which is a zero mean additive white Gaussian noise (AWGN):

$$\begin{aligned} \widehat{\phi}_{max,F_{c1}} &= \phi_{max,F_{c1}} + n_{F_{c1}} \\ \widehat{\phi}_{max,F_{c2}} &= \phi_{max,F_{c2}} + n_{F_{c2}} \end{aligned} \tag{19}$$

where $n_{F_{c1}}$ and $n_{F_{c2}}$ represent the contribution of noise to the phase measurements. This noise impairs the precision of the path difference estimate on the OFDM signals:

$$\begin{aligned} (\widehat{d_2 - d_1})_{F_{c1,a}} &= \frac{\lambda_1}{2\pi}(\phi_{max,F_{c1}} + n_{F_{c1}}) \\ (\widehat{d_2 - d_1})_{F_{c2,a}} &= \frac{\lambda_2}{2\pi}(\phi_{max,F_{c2}} + n_{F_{c2}}) \end{aligned} \tag{20}$$

where the subscript a is used to emphasize that the path differences are affected by ambiguity. The variances of the two estimates are:

$$\sigma^2_{F_{c1}} = \left(\frac{\lambda_1}{2\pi}\right)^2 \sigma^2 \quad \sigma^2_{F_{c2}} = \left(\frac{\lambda_2}{2\pi}\right)^2 \sigma^2 \tag{21}$$

where σ^2 is the noise variance. The noise effect is even more destructive in the case of the *wide-lane* technique:

$$(\widehat{d_2 - d_1})_{F_{wl}} = \frac{\lambda_{wl}}{2\pi}(\phi_{max,F_{c2}} + n_{F_{c2}} - \phi_{max,F_{c1}} - n_{F_{c1}}) \tag{22}$$

where the noise variance is not only doubled because of subtraction but also scaled with a higher factor $\lambda_{wl}/2\pi$:

$$\sigma^2_{wl} = \left(\frac{\lambda_{wl}}{2\pi}\right)^2 2\sigma^2 \tag{23}$$

C. PHASE AMBIGUITY RESOLUTION BY HALF-CYCLE ROUNDING

In this section we propose an approach that significantly improves the precision of the path difference estimation by *wide-lane* technique. We start from the observation that if the half-wavelength condition (16) is not satisfied, then the true path difference $\widehat{d_2 - d_1}$ is composed of a fractional number of half-cycles measured from the cross-correlation phase and an integer number of half-cycles M that is unknown:

$$\widehat{d_2 - d_1} = M_2 \frac{\lambda_2}{2} + (\widehat{d_2 - d_1})_{F_{c2},a} \tag{24}$$

The higher frequency F_{c2} (corresponding to the lower wavelength λ_2) has been considered in order to have a reduced noise scaling (see (21)). Unfortunately, the estimation based on (24) cannot be used because of M_2. The problem of M_2 is alleviated by the *wide-lane* technique, where the half-wavelength condition is satisfied ($M_{wl} = 0$):

$$\widehat{d_2 - d_1} = (\widehat{d_2 - d_1})_{F_{wl}} \tag{25}$$

The drawback of the *wide-lane* measurement is the increased noise with respect to (24).

In our approach, instead of deriving the path difference directly from the *wide-lane* phase, we estimate solely the integer M_2 by using the *wide-lane* technique and then we obtain $\widehat{d_2 - d_1}$ with (24). To get an estimate of M_2, we substitute (25) in (24):

$$(\widehat{d_2 - d_1})_{F_{wl}} = M_2 \frac{\lambda_2}{2} + (\widehat{d_2 - d_1})_{F_{c2},a} \tag{26}$$

and perform a rounding operation since M_2 is always an integer:

$$\widehat{M_2} = round\left[\frac{(\widehat{d_2 - d_1})_{F_{wl}} - (\widehat{d_2 - d_1})_{F_{c2},a}}{\frac{\lambda_2}{2}}\right] \tag{27}$$

The rounding is the key for increasing the precision of $\widehat{d_2 - d_1}$. Once M_2 estimated, the actual path difference can be obtained with (24). The rest of the section is devoted to the evaluation of the precision of the $\widehat{d_2 - d_1}$ estimator.

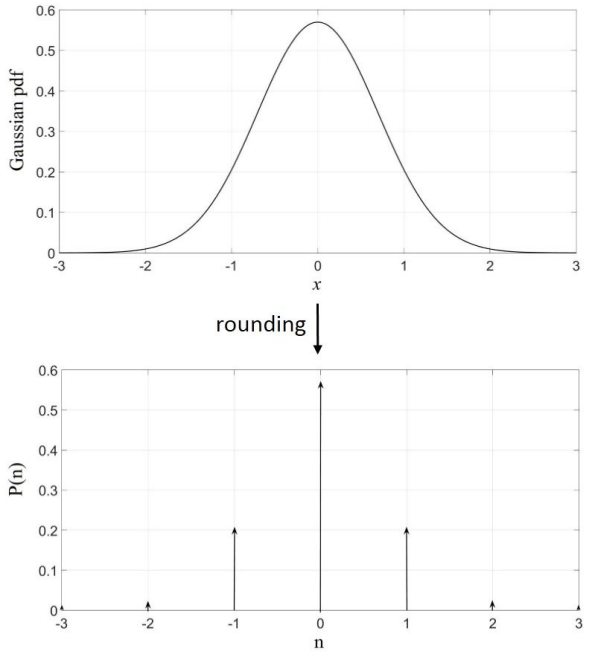

FIGURE 7. Distribution of n_{M_2} before (top) and after the rounding of M_2 (bottom).

According to (24) the variance of the *wide-lane* estimator is the weighted sum of two terms, $\sigma^2_{F_{c2}}$ and $\sigma^2_{M_2}$. The noise associated to M_2 before rounding is:

$$n_{M_2} = \frac{\frac{\lambda_{wl}}{2\pi}(n_{F_{c2}} - n_{F_{c1}}) - \frac{\lambda_2}{2\pi}n_{F_{c2}}}{\frac{\lambda_2}{2}} = \frac{1}{\pi}\left(\frac{F_{c2}}{F_{c2}-F_{c1}}n_{F_{c1}} + \frac{F_{c1}}{F_{c2}-F_{c1}}n_{F_{c2}}\right) \quad (28)$$

and consequently, the variance of M_2 estimator before rounding is:

$$\sigma^2_{M_2} = \frac{\sigma^2}{\pi^2}\frac{F^2_{c2}+F^2_{c1}}{(F_{c2}-F_{c1})^2} \quad (29)$$

The noise n_{M_2} is as $n_{F_{c2}}$ an AWGN with zero mean.

The rounding of M_2 changes the noise distribution into a series of Dirac (Fig. 7) with the amplitudes:

$$P(n) = \int_{n-0.5}^{n-0.5} \frac{1}{\sqrt{2\pi}\sigma_{M_2}} e^{-\frac{x^2}{2\sigma^2_{M_2}}} dx \quad (30)$$

The integral is the probability to obtain n after rounding. The variance of the distribution after rounding is:

$$\sigma^2_{[M_2]} = 2\sum_{n=1}^{\infty} n^2 P(n) \quad (31)$$

For high $\sigma^2_{M_2}$, the rounding has almost no influence on the noise variance that remains practically the same. The plot in Fig. 8 shows the ratio between the noise standard deviation after and before rounding. Note how close it is to 1 for $\sigma_{M_2} > 1.5$. On the contrary, for low $\sigma^2_{M_2}$, when the Gaussian

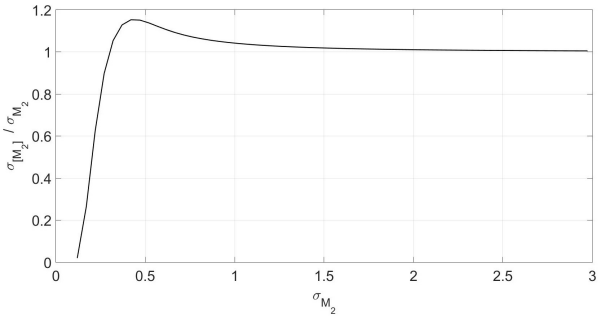

FIGURE 8. The ration between the noise standard deviation after rounding and before rounding. For $\sigma_{M_2} < 0.3$ the rounding reduces the noise variance.

is tightened about zero, the rounding may reduce significantly the variance, as shown in Fig. 8. This is the case of our application, where $\sigma^2_{M_2}$ is in the range of 10^{-3}.

To calculate the infinite sum in (31), we start from the following approximation:

$$n^2 \int_{n-0.5}^{n+0.5} \frac{1}{\sqrt{2\pi}\sigma_{M_2}} exp(-\frac{x^2}{2\sigma^2_{M_2}})dx \approx \int_{n-0.5}^{n+0.5} x^2 \frac{1}{\sqrt{2\pi}\sigma_{M_2}} exp(-\frac{x^2}{2\sigma^2_{M_2}})dx \quad (32)$$

that holds for Gaussian distributions with low variance. In such cases, in the intervals $[n-0.5, n+0.5]$ the Gaussian is almost constant, meaning that the above approximation is equivalent to:

$$n^2 \approx \int_{n-0.5}^{n+0.5} x^2 dx = n^2 + 0.08 \quad (33)$$

By using (32), the variance after rounding can be approximated by:

$$\sigma^2_{[M_2]} \approx 2\int_{0.5}^{\infty} x^2 \frac{1}{\sqrt{2\pi}\sigma_{M_2}} exp(-\frac{x^2}{2\sigma^2_{M_2}})dx \quad (34)$$

The calculation of the integral leads to the following expression for the variance:

$$\sigma^2_{[M_2]} = \sigma^2_{M_2}\left[1 - erf\left(\frac{1}{2\sqrt{2}\sigma_{M_2}}\right)\right] + \frac{\sigma_{M_2}}{\sqrt{2\pi}} e^{-\frac{1}{8\sigma^2_{M_2}}} \quad (35)$$

where $erf(x)$ is the error function.

Table 1 shows the variance of M_2 calculated for $F_{c1} = 1.1$ GHz, $F_{c2} = 1.2$ GHz, $r = 18.75$ cm (conservative value considering the physical dimensions of the satellite) and σ^2 corresponding to a SNR of 10 dB. It is to note that after applying HCR the variance of M_2 is reduced by 9 orders of magnitude. It becomes practically zero, meaning that by HCR the unambigous *wide-lane* estimation of path difference becomes as precise as the ambigous estimation on a single channel.

The direct consequence of improving the path difference estimation is a more accurate measurement of α. Fig. 9 shows the standard deviation of α vs. SNR in two cases: calculated

TABLE 1. Estimator variance at 10 dB.

$\sigma^2[rad^2]$	$\sigma^2_{F_{c2}}[m^2]$	$\sigma^2_{wl}[m^2]$	$\sigma^2_{M_2}$	$\sigma^2_{[M_2]}$	$\sigma_\alpha[^\circ]$
$2.1e-4$	$3.3e-7$	$9.5e-5$	$5.6e-3$	$5.1e-12$	0.088

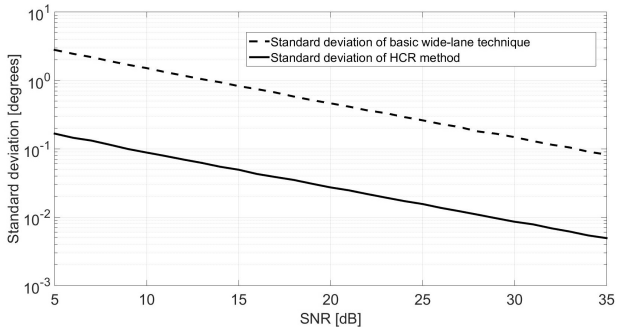

FIGURE 9. Standard deviation of α vs. SNR calculated with the basic *wide-lane* tehnique and by HCR (MATLAB simulations). The values were obtained from 5000 runs at each SNR.

TABLE 2. Standard deviation of α vs. DFT size at 10 dB.

DFT size	256	512	1024	2048
Subcarriers modulated	150	300	600	1200
σ_α [degrees]	0.1248	0.0883	0.0625	0.0443

with $\widehat{d_2 - d_1}$ estimated with the basic *wide-lane* technique and estimated by HCR. At 10 dB, the precision is improved from 1.467° to 0.088°.

Another possibility to improve the precision of α is by increasing the number of modulated subcarriers in the OFDM symbol and, consequently, the DFT size. The calculus of correlation reduces the noise σ associated to ϕ_{max}. The noise reduction is more consistent as the number of transmitted subcarriers increases. Table 2 shows the values of σ_α for DFT sizes and corresponding number of modulated subcarriers at a SNR of 10 dB. The values for r, F_s and F_{c2} are the same as for Table 1. The subcarrier spacing is modified in order to have the same signal bandwidth regardless of DFT size. It can be seen that the error reduction by doubling DFT size is approximately $1/\sqrt{2}$, which corresponds to doubling the number of modulated subcarriers. The precision obtained for a 512 point DFT is consistent with the result obtained in Table 1.

IV. OTHER SOURCES OF ERRORS

Several sources of errors have been identified in inter-satellite communications. The effects of the misalignment between transmitter and receiver oscillators and multipath propagation are discussed in the following subsections.

Another potential impairment is oscillator phase noise, which has two effects on the received signal: a common phase error (CPE) among subcarriers [38] and intercarrier interference (ICI) [39]. Since on a satellite platform the same oscillator would be shared by all receivers, CPE does not influence the AoA estimation due to the specific measurement technique by cross-correlation (which translates to pointwise multiplication of spectra). We performed simulations that integrate both effects of phase noise considering the specifications of the oscillator [40] in the Octoclock device [41] that is used in the USRP testbed. For the AoA range simulated in the testbed, the error was under 0.0002°.

Rain [42] and shadow fading [43] are specific to satellite-ground communications and do not affect ISLs. The ionospheric delay does not impact our technique since the AoA measurement is based on path difference estimation of the received signals. Furthermore, the change in AoA due to ionospheric scintillation is also negligible [44].

A. EFFECTS OF CARRIER FREQUENCY OFFSET

In inter-satellite communications, the differences between the local oscillators of the transmitter and receiver and the Doppler effect give rise to a shift in the frequency domain. This shift is referred to as *carrier frequency offset* (CFO). In OFDM, the demodulation of a signal with an offset in the carrier frequency leads to orthogonality loss, ICI and finally to large bit error rates. Therefore, any transmission has to be preceded by a synchronization process. During synchronization, the CFO is estimated and corrected, but since the estimation is prone to errors, even after the correction a residual CFO is still present. The residual offset Δf_c can be modelled as a multiplicative distortion in time domain [45]:

$$y_{CFO}(t) = y(t)e^{j2\pi t\Delta f_c} \tag{36}$$

In section III-B we have shown that in most cases the maximum measured for the correlation is not the actual correlation peak, but a value $R(\tau)$ (with $\tau < T_s/2$) in its vicinity. The CFO contributes to the phase of this value:

$$\begin{aligned} R_{CFO}(\tau) &= \int_0^{NT-1} y_1(t+\tau)e^{j2\pi(t+\tau)\Delta f_c} \\ y_2^*(t)e^{-j2\pi t\Delta f_c}dt &= e^{j2\pi\tau\Delta f_c}R(\tau) \end{aligned} \tag{37}$$

Equation (37) shows that the CFO introduces an error in correlation phase measurement that is equal with the product $2\pi\Delta f_c\tau$. This error biases the AoA estimation by approximately:

$$bias_\alpha = arcsin\left(\frac{\lambda_c}{4\pi r}2\pi\tau\Delta f_c\right) \approx \frac{\lambda_c}{2r}\Delta f_c\tau \tag{38}$$

The variation of the bias for different values of F_s are shown in Fig. 10. The residual CFO is in the range [1, 100] Hz, which is representative considering the synchronization accuracy in LTE systems [46]. In [46] the SNR is in the range $[-20, -10]$ dB, therefore the residual CFO range is more than sufficient for our application. For $\Delta f_c = 38$ Hz, a sampling frequency $F_s = 7.68$ MHz, $F_c = 1.2$ GHz and $r = 18.75$ cm, the bias is in the most unfavourable case ($\tau = T/2$) equal to $9 \cdot 10^{-5}$ degrees. It is a negligible value.

B. EFFECTS OF MULTIPATH PROPAGATION

In the case of inter-satellite communications, the main sources of multipath propagation are the reflections of the

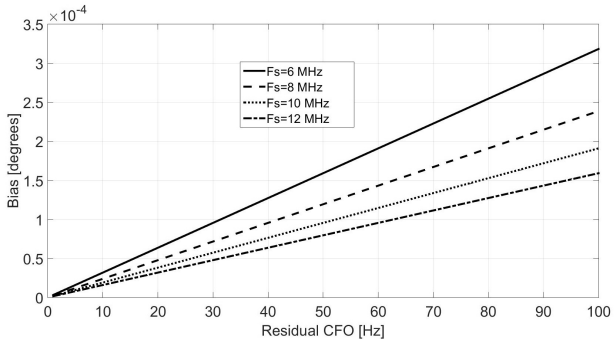

FIGURE 10. AoA estimation bias vs. residual CFO when $\tau = T/2$ (results obtained by MATLAB simulations).

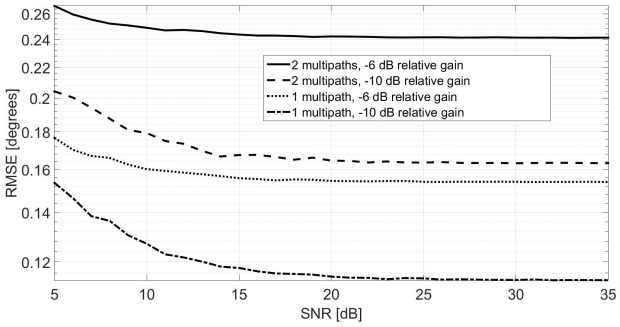

FIGURE 11. RMSE of α estimated by HCR vs. SNR in 4 multipath scenarios. For simulation, 3000 runs were performed at each SNR.

RF signal on the structure surrounding the antennas [47]. Because the distance between the two receiver antennas Rx1 and Rx2 is negligible compared to the inter-satellite distance, multipath propagation coming from the slave satellite can be assumed to be identical for both paths. At the master satellite, this is no longer the case. The characteristics of multipath vary with the relative orientation of the satellites.

The channel impulse response of a wireless channel can be expressed as [48]:

$$h[n] = \sum_{l=0}^{L-1} a_l \delta[n - \tau_l] \tag{39}$$

where τ_l is the delay of the lth path, a_l is the corresponding complex path gain and L is the total number of channel paths. For simplicity, it is assumed that the channel is linear-time invariant and slowly fading. In multipath conditions, the received signal can be modelled as:

$$y_{mp}[n] = x[n] * h[n] = \sum_{l=0}^{L-1} h[n]x[n - l] \tag{40}$$

The use of the cyclic prefix (CP) allows the multipath propagation to be modeled as pointwise multiplication in the frequency domain [49]:

$$Y_{mp}[k] = X[k]H[k] \tag{41}$$

where $Y_{mp}[k]$ is the DFT of the received signal and $H[k]$ is the channel transfer function. With this model, the spectrum of $R(\tau)$ becomes:

$$\begin{aligned}\mathcal{F}\{R_{mp}(\tau)\} &= Y_{1,mp}[k]Y^*_{2,mp}[k] \\ &= |X|^2 H_1[k]H_2^*[k]e^{j2\pi \frac{d_2-d_1}{c} F_c} e^{j2\pi \frac{d_2-d_1}{c} k \frac{F_s}{N}}\end{aligned} \tag{42}$$

This equation shows how multipath propagation influences the phase measurements. The error can be up to several cm in path difference and could lead to ambiguity resolution failure and degradation of accuracy [47]. A potential solution for this issue is multipath error mapping in an anechoic chamber using satellite mock-ups, as performed in PRISMA mission [50].

Fig. 11 shows the root mean square error (RMSE) values in the estimation of α by HCR for several multipath scenarios obtained via simulations. The same parameters as in section III-A are used. Additionally we set $\alpha = 10°$ and $y = 25$ m. Four cases are considered: one and two secondary paths with -6 dB relative gain, one and two secondary paths with -10 dB relative gain. The relative delays of the multipath signals are set to correspond to reflections on the surfaces surrounding the satellite antennas. The plots show that regardless of scenario, the accuracy of α reaches a plateau after certain SNR values. As expected, higher attenuation of the multipaths leads to lower errors. In the cases of two multipaths, at a SNR of 10 dB, the RMSE is 0.249° and 0.179°, respectively. After a SNR of 25 dB, the RMSE is fairly constant at 0.241° and 0.163°. If only one multipath is considered, at a SNR of 10 dB the RMSE values are 0.16° and 0.127° and the plateau values are 0.154° and 0.113°, respectively. However, a realistic characterization of the multipath propagation cannot be performed until the properties of the structure surrounding the satellite's antennas are known.

V. EXPERIMENTAL RESULTS

In the previous sections, a series of theoretical considerations have been done regarding the AoA estimation. In this section, part of them are validated by tests on an ISL implemented in real-time using NI-USRP 2952R platforms [51]. The USRP is a scalable software defined radio platform for designing and deploying wireless communications systems. It has a user-programmable Kintex-7 FPGA and two radio frequency channels RF0 and RF1 with the RF front-end provided by two daughterboards. Each daughterboard has two available ports: one that can be set either as transmitter or receiver, and another that can be used only as a receiver. The USRPs are programmed in the LabVIEW Communications environment [52] and are connected to host PCs via PCIe cables.

A. ISL IMPLEMENTATION

The ISL is implemented using Time Division Duplexing (TDD) with a frame structure of 10 ms as shown in Fig. 12. The frame is divided in two equal subframes.

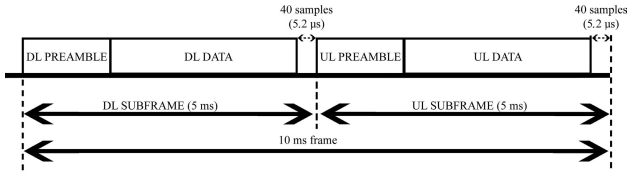

FIGURE 12. Structure of the TDD frame used in the implementation of the ISL.

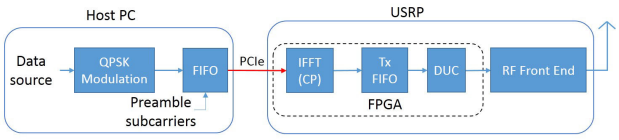

FIGURE 13. Transmitter chain of the ISL implementation.

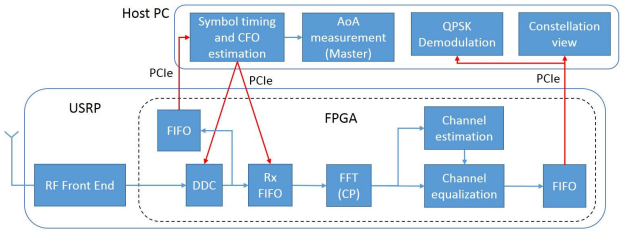

FIGURE 14. Receiver chain of the ISL implementation.

The first one is the Downlink (DL), used to send data from the master to the slave, the other one is the Uplink (UL) reserved for sending data in the reverse sense. The Transmit/Receive Transition Gap (TTG) and the Receive/Transmit Transition Gap (RTG) are set to 5.2 µs, long enough to accommodate the round trip delay.

For an OFDM symbol, the DFT size is 512 and the length of the CP is 36 samples, leading to a total symbol length of 548 samples. From the total of 511 subcarriers, the first 106 constitute the lower guard band, the next 300 are data subcarriers and the last 105 form the upper guard band. The data subcarriers are QPSK-modulated. The sampling frequency is set to 7.68 MHz, which leads to a total of 70 symbols for each subframe. The resulting bandwidth of 4.5 MHz (correlated with the modulation scheme) is sufficient to accommodate the data rate for typical ISL payloads [4]. The subframes start with a preamble symbol, specific to either the DL or UL. The 300 data subcarriers of the preamble are modulated by a pseudorandom QPSK sequence that is different for the DL and UL subframes.

The master satellite provides the time base for the ISL, thus time and frequency synchronization are performed at the slave. The time synchronization is achieved using the cross-correlation technique that provides precise timing offset estimation. It is followed by CFO estimation and correction. The phase measurements for the AoA estimation are initiated at the master after synchronization.

The block diagram of the transmitter chain of the ISL is shown in Fig. 13. On the host PC, the stream of data is modulated using a QPSK scheme and is sent along with the preamble subcarriers through a First In First Out (FIFO) towards the FPGA of the USRP. The PC and FPGA communicate using a PCIe connection. On the FPGA, the IFFT block has the following roles: on a symbol-by-symbol basis it is used to modulate the data subcarriers, add the guard subcarriers, perform the inverse FFT and then add the CP. The time-domain samples are sent via the Tx FIFO to the Digital Upconverter (DUC) which interpolates the signal and performs I/Q modulation. The I/Q data is forwarded towards the RF front end.

The receiver processing chain is depicted in Fig. 14. The Digital Downconverter (DDC) receives I/Q data from the RF front end and decimates the signal. The time-domain samples are sent through another FIFO to the symbol timing and CFO estimation block on the PC. This block has different purposes at each satellite. At the slave, it estimates frame timing and CFO and sends the correction values to the FPGA to adjust the phase in the DDC (for CFO compensation) and the timing of the Tx and Rx FIFOs. At the master, this block is used only to estimate the beginning of the UL and adjust the timing of the Rx FIFO accordingly. After synchronization, the received symbols are subject to CP removal and FFT transform in the FFT block. For each radio frame, the preamble subcarriers are used for channel estimation (least-squares technique). The subcarriers of the data symbols are equalized and then sent via another FIFO to the host for constellation view and QPSK demodulation. The slave begins transmitting data only after time-frequency synchronization is completed.

The AoA is estimated on the host PC of the master satellite using the received preambles. The LabVIEW Communications block diagram used to implement the measurement is shown in Fig. 15. The cross-correlation phases are measured on both frequencies, the *wide-lane* combination is taken and then the ambiguity is resolved in the HCR sub-block.

ITU regulations specify that L and S bands are the only frequency bands below 10 GHz which can be used for space-to-space communications [53]. Thus, an S band frequency would be desirable to reduce the influence of noise on the phase measurements (see (21)). For our experiment, the RF spectrum was scanned using a spectrum analyzer and two central frequencies in the L-band, $F_{c1} = 1.1$ GHz and $F_{c2} = 1.2$ GHz, were chosen such that interference from other radio transmissions is minimized. The data communication link is on the first frequency, while only the preamble is transmitted on the second frequency for AoA estimations. The payload usually consists of various sensor measurements and satellite health data. The *wide-lane* combination of F_{c1} and F_{c2} leads to $\lambda_{wl} = 3$ m.

B. THE USRP TESTBED

The setup consists of three NI-USRP 2952R platforms, as can be seen in Fig. 16. USRP 1 and USRP 2 are used to implement the master satellite and USRP 3 to implement the slave

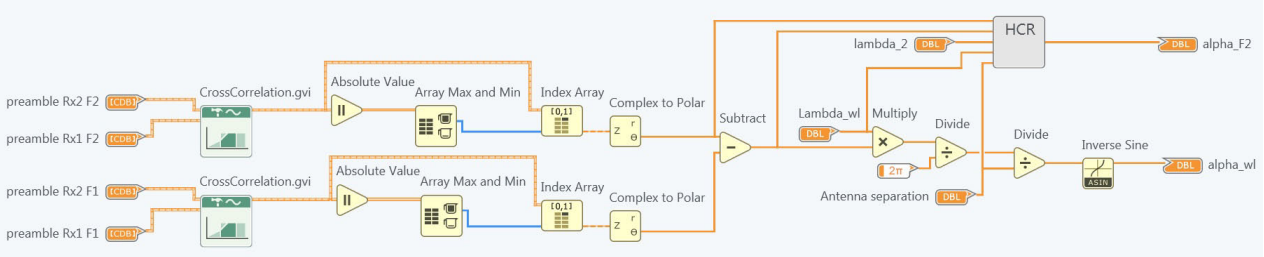

FIGURE 15. LabVIEW Communications block diagram of the AoA measurement process.

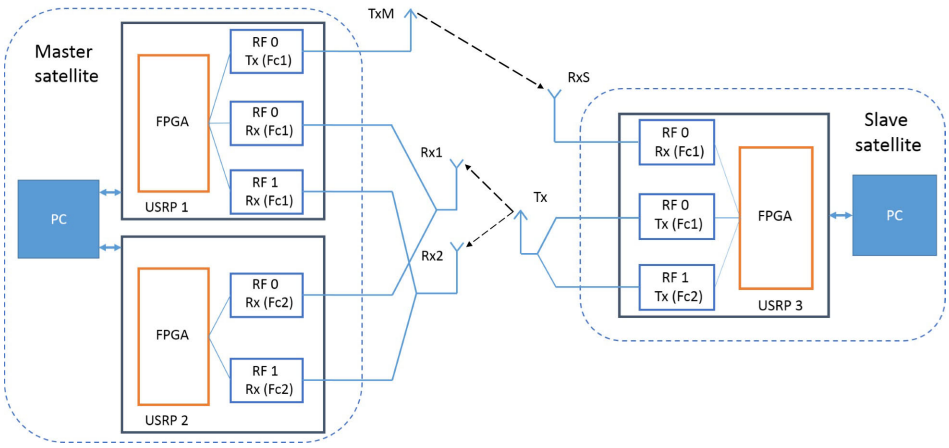

FIGURE 16. Diagram of the experimental setup: the Master Satellite is implemented with two USRPs that supply the 4 receiver channels necessary for the *wide–lane* technique, while for the slave satellite a single USRP is sufficient. The USRPs are controlled by PCs via PCIe cables and interfaces.

satellite. The two USRPs at the master satellite are demanded by the *wide–lane* technique. At the master, USRP 1 is tuned to F_{c1} and USRP 2 is tuned to F_{c2}. The Rx1 antenna is connected to the RF0 receiver channels of both USRPs and Rx2 is connected to the RF1 receiver channels. The cables that connect the receiver antennas to the USRPs are of equal length. The TxM antenna is connected to RF0's transmitter channel on USRP1 and streams data towards the slave.

At the slave satellite, the transmitter channel of RF0 is tuned to F_{c1} and the transmitter channel of RF1 to F_{c2}. These two transmitters are connected to the Tx antenna. Only one receiver channel is needed at the slave, it is tuned at F_{c1} and connected to the RxS antenna. Splitters/combiners are used whenever multiple ports must be connected to the same antenna.

For the purpose of the real-time measurements, the reference frequency is generated externally by an Octoclock device and is provided to all three USRPs using coaxial cables. The USRPs are controlled by PCs at each terminal using PCIe cables and interfaces.

To implement different values for α, the antennas of the master satellite are mounted on a tripod which has a rotatable surface on top. A picture of the setup is in Fig. 17. The rotation can be performed with a step of 2° in the range $[-30°, +30°]$. The distance between Rx1 and Rx2 is 37.5 cm, meaning that

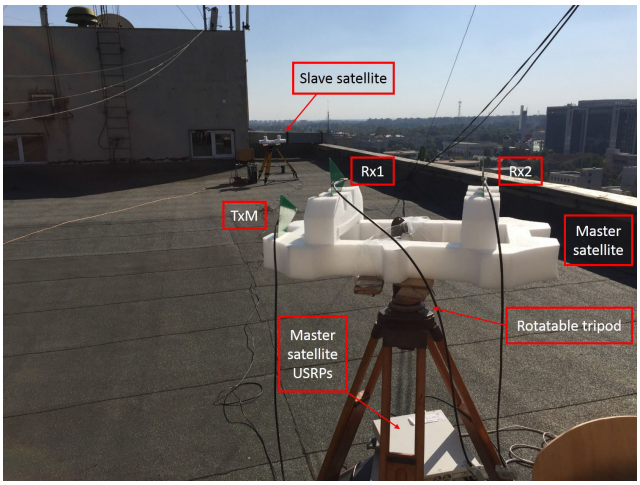

FIGURE 17. Experimental testbed for AoA estimation mounted on top of the faculty of electronics, telecommunications and information technology in bucharest.

λ_{wl} fulfils the half-wavelength condition. In our experiment all antennas are placed at the same height.

C. RESULTS ON MEASURED DATA

We considered two scenarios: in the first one, the transmit power of the satellites is set such to obtain a SNR of 26 dB and

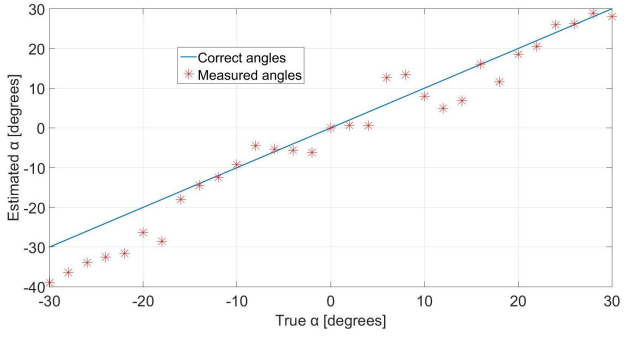

FIGURE 18. AoA estimated with the basic *wide-lane* technique and real-time measurements at SNR = 26 dB. The correct values of the angles are represented by the full line.

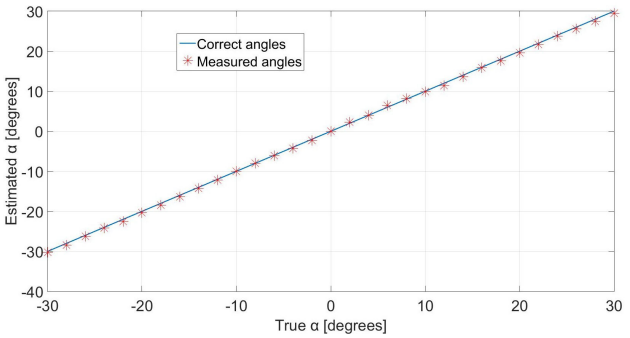

FIGURE 19. AoA estimated by HCR from real-time measurements at SNR = 26 dB. The correct values of the angles are represented by the full line.

α is varied from $-30°$ to $30°$ with a step of $2°$. In the second scenario, α is set at $10°$ and the transmit power is tuned such to have SNR values from 5 to 35 dB. In both scenarios, we start by a calibration stage consisting in the following steps: we verify by physical measurements that d_1 and d_2 are equal, we rotate the tripod such to indicate $\alpha = 0$ and we measure the phases at the maximum of the correlation on F_{c1} and F_{c2}. The path difference Δd calculated with (24) will serve to correct all further measurements. This calibration process is required by our setup because the USRP phase locked loops (PLL) have random initial phases. In a real scenario, with satellites implemented on different hardware platforms where the PLL phases are deterministic and multi-chip phase synchronization is supported (such as [54]), this calibration is not required.

Regardless of the considered scenario, the procedure for measuring the angle α has been the following:

1) The phases are measured at the maximum of the correlation on both F_{c1} and F_{c2};
2) The path difference is estimated either with (22) or (24);
3) The path difference is corrected by subtracting Δd;
4) The AoA α is calculated with (7).

Fig. 18 depicts the angles estimated in the first scenario with the basic *wide-lane* technique at 26 dB. For the same phase measurements, the angles estimated by HCR are shown in Fig. 19. In this plot, the dots are much closer to the ideal straight-line, showing a more accurate estimation.

In the second secenario, with α set at $10°$, the transmit power at the slave is varied such to obtain 10 different SNRs. For each SNR, 5000 phase measurements (5000 frames) on F_{c1} and 5000 on F_{c2} are recorded and for each couple of measurements two values are calculated for α, one with the basic *wide-lane* technique and the other by HCR. Based on the 2×5000 measurements, we have calculated the standard deviation of each estimator (Fig. 20). The real-time results are close to the simulated values, aiding in the validation of our approach. The precision provided by HCR remains more than one order of magnitude better than that obtained by the the basic *wide-lane* technique. For instance, at 10 dB

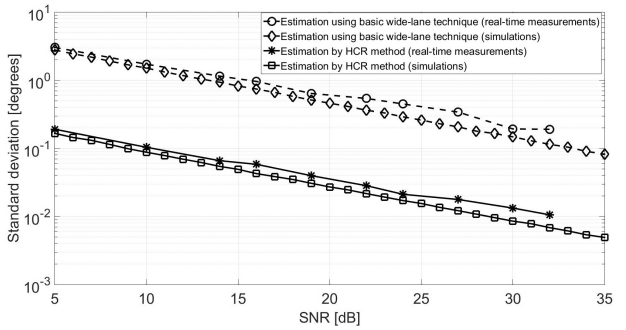

FIGURE 20. AoA standard deviation with real-time measurements (dotted lines) and by simulations (solid lines). For the real-time measurements, the ten SNR values represented with markers were obtained by varying the transmit power at the slave satellite. 5000 measurements were performed at each SNR.

SNR the precision is improved from $1.728°$ to $0.104°$. The gap is similar to what was obtained by simulations, where the improvement has been from $1.467°$ to $0.088°$. For noise levels superior to 16 dB, the standard deviation of the real-time measurements is under $0.06°$.

These results are in the range of $1°$ precision obtained in PRISMA and are comparable to the performances reported for GPS based systems. For instance, in [55] accuracies between $0.1°$ and $0.2°$ were achieved in a system consisting in 3 GPS receivers and phase ambiguity resolution resolved by LAMBDA and LSAST algorithms. The Multivariate Constrained LAMBDA in [56] provides accuracies between $0.054°$ and $0.186°$. Our approach could be further improved by increasing the distance between the receiver antennas if the satellite dimensions allow it.

We also tested the effect of CFO on HCR estimator by simulating a small residual CFO between the master and slave. To this end, a separate signal generator was used to supply the reference frequency for the slave satellite. Its frequency was set such that the CFO at 1.2 GHz is roughly 38 Hz. The same measurements as in the first scenario were done (Fig. 21). No significant difference was discerned between the cases with and without CFO.

A realistic evaluation of multipath propagation for our system could be done only by knowing the satellite structure

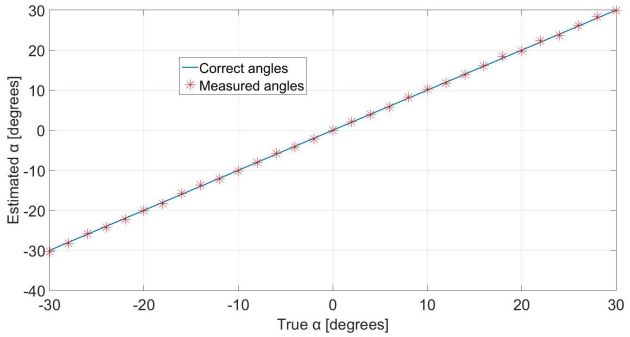

FIGURE 21. AoA estimated by HCR at SNR = 26 dB and a residual CFO of 38 Hz. The correct values of AoA are represented by the full line. (Results obtained with real-time measurements).

and by using an anechoic chamber as in PRISMA. The technological level of our experiment did not permit such an investigation.

VI. CONCLUSION

The paper proposes an RF method for AoA estimation by using the preamble of an OFDM ISL. The ambiguity in path difference measurement is resolved by an improved method (HCR) that reduces the standard deviation of the AoA estimator by an order of magnitude. The influence of several parameters and factors is analyzed: sampling frequency, receiver noise, DFT size, CFO and multipath propagation. They are evaluated separately by simulations and jointly by measurements on a testbed implemented with USRPs. The simulations with realistic parameters show that the sampling frequency and the CFO introduce very low biases in the AoA estimation. These biases are in the range of 10^{-3} and 10^{-4} degrees, respectively. For SNR values above 10 dB the AoA standard deviation is less than 10^{-1} degrees. The highest errors are introduced by multipath propagations. The simulations with one and two secondary paths show biases up to 0.26° for the considered parameters.

The real-time measurements with the testbed are close to the results obtained by simulations and confirm the improvement in precision due to HCR. The overall precision of AoA estimation is comparable with that of other RF methods in the literature but remains in the low range of dedicated attitude sensors. It can be improved by increasing the DFT size and the antenna separation if allowed by the satellite dimensions.

REFERENCES

[1] K. An, T. Liang, X. Yan, and G. Zheng, "On the secrecy performance of land mobile satellite communication systems," *IEEE Access*, vol. 6, pp. 39606–39620, 2018. doi: 10.1109/ACCESS.2018.2854233.

[2] K. An, J. Ouyang, M. Lin, and T. Liang, "Outage analysis of multi-antenna cognitive hybrid satellite-terrestrial relay networks with beamforming," *IEEE Commun. Lett.*, vol. 19, no. 7, pp. 1157–1160, Jul. 2015. doi: 10.1109/LCOMM.2015.2428256.

[3] F. Guidolin, M. Nekovee, L. Badia, and M. Zorzi, "A study on the coexistence of fixed satellite service and cellular networks in a mmWave scenario," in *Proc. IEEE Int. Conf. Commun. (ICC)*, London, U.K., Jun. 2015, pp. 2444–2449. doi: 10.1109/ICC.2015.7248691.

[4] R. Radhakrishnan, W. W. Edmonson, F. Afghah, R. M. Rodriguez-Osorio, F. Pinto, and S. C. Burleigh, "Survey of inter-satellite communication for small satellite systems: Physical layer to network layer view," *IEEE Commun. Surveys Tuts.*, vol. 18, no. 4, pp. 2442–2473, 4th Quart., 2016. doi: 10.1109/COMST.2016.2564990.

[5] J. S. Llorente, A. Agenjo, C. Carrascosa, C. de Negueruela, A. Mestreau-Garreau, A. Cropp, and A. Santovincenzo, "PROBA-3: Precise formation flying demonstration mission," *Acta Astron.*, vol. 82, no. 1, pp. 38–46, Jan. 2013. doi: 10.1016/j.actaastro.2012.05.029.

[6] J. Harr, M. Delpech, L. Lestarquit, and D. Seguela, "RF metrology validation and formation flying demonstration by small satellites—The CNES participation on the PRISMA mission," in *Proc. 4th Symp.*, Sardinia, Italy, Nov. 2006, pp. 1–10.

[7] S. Persson, S. Veldman, and P. Bodin, "PRISMA—A formation flying project in implementation phase," *Acta Astron.*, vol. 65, pp. 1360–1374, Nov./Dec. 2009. doi: 10.1016/j.actaastro.2009.03.067.

[8] S. Roose, Y. Stockman, and Z. Sodnik, "A lateral sensor for the alignment of two formation-flying satellites," in *Proc. 5th Int. Conf. SFFMT*, Berlin, Germany, May 2013.

[9] M. Bradshaw, Y. Gao, K. Homewood, L. Gagnon, and S. Gagnon, "Fine lateral and longitudinal sensor (FLLS) on-board ESA'S PROBA-3 mission," in *Proc. IAC*, Adelaide, SA, Australia, Sep. 2017, pp. 1–7.

[10] M. Delpech, P.-Y. Guidotti, T. Grelier, and J. Harr, "RF based navigation for PRISMA and other formation flying missions in earth orbits," in *Proc. ISSFD*, Paris, France, Oct. 2009.

[11] *PROBA-3 Mission*. Accessed: Dec. 5, 2018. [Online]. Available: https://directory.eoportal.org/web/eoportal/satellite-missions/p/proba-3

[12] Y. G. Li and G. L. Stuber, *Orthogonal Frequency Division Multiplexing for Wireless Communications*. New York, NY, USA: Springer, 2006, pp. 199–241.

[13] A.-M. Crisan, A. Martian, and D. Coltuc, "Relative orientation estimation in formation flying satellites," in *Proc. IEEE ISSCS*, Jul. 2017, pp. 1–4. doi: 10.1109/ISSCS.2017.8034927.

[14] P. Gupta, K. Aditya, and A. Datta, "Comparison of conventional and subspace based algorithms to estimate direction of arrival (DOA)," in *Proc. IEEE ICCSP*, Melmaruvathur, India, Apr. 2016, pp. 251–255. doi: 10.1109/ICCSP.2016.7754133.

[15] A. Massoud and A. Noureldin, "Angle of arrival estimation based on warped delay-and-sum (WDAS) beamforming technique," in *Proc. OCEANS*, Waikoloa, HI, USA, Sep. 2011, pp. 1–4. doi: 10.23919/OCEANS.2011.6107316.

[16] J. Capon, "High-resolution frequency-wavenumber spectrum analysis," *Proc. IEEE*, vol. 57, no. 8, pp. 1408–1418, Aug. 1969. doi: 10.1109/PROC.1969.7278.

[17] E. Khan and D. T. M. Slock, "Direction of arrival estimation using quadratic time frequency distributions," in *Proc. 21st IST Mobile Wireless Commun.*, Lisbon, Portugal, 2003, pp. 1–5.

[18] R. G. Lorenz and S. P. Boyd, "Robust minimum variance beamforming," *IEEE Trans. Signal Process.*, vol. 53, no. 5, pp. 1684–1696, May 2005. doi: 10.1109/TSP.2005.845436.

[19] S.-F. Chuang, W.-R. Wu, and Y.-T. Liu, "High-resolution AoA estimation for hybrid antenna arrays," *IEEE Trans. Antennas Propag.*, vol. 63, no. 7, pp. 2955–2968, Jul. 2015. doi: 10.1109/TAP.2015.2426795.

[20] P. Vallet, X. Mestre, and P. Loubaton, "Performance analysis of an improved MUSIC DoA estimator," *IEEE Trans. Signal Process.*, vol. 63, no. 23, pp. 6407–6422, Dec. 2015. doi: 10.1109/TSP.2015.2465302.

[21] Y. P. Liao and A. Abouzaid, "Resolution improvement for MUSIC and ROOT MUSIC algorithms," *J. Inf. Hiding Multimedia Signal Process.*, vol. 6, no. 2, pp. 189–197, Mar. 2015.

[22] P. Charge, Y. Wang, and J. Saillard, "An extended cyclic MUSIC algorithm," *IEEE Trans. Signal Process.*, vol. 51, no. 7, pp. 1695–1701, Jul. 2003. doi: 10.1109/TSP.2003.812834.

[23] M. Jalali, M. N. Moghaddasi, and A. Habibzadeh, "Comparing accuracy for ML, MUSIC, ROOT-MUSIC and spatially smoothed algorithms for 2 users," in *Proc. MMS*, Tangiers, Morocco, Nov. 2009, pp. 1–5. doi: 10.1109/MMS.2009.5409832.

[24] T. S. Dhope, "Application of MUSIC, ESPRIT and ROOT MUSIC in DOA estimation," Fac. Elect. Eng. Comput., Univ. Zagreb, Zagreb, Croatia, Tech. Rep., 2010. [Online]. Available: https://www.semanticscholar.org

[25] R. Roy and T. Kailath, "ESPRIT-estimation of signal parameters via rotational invariance techniques," *IEEE Trans. Acoust., Speech, Signal Process.*, vol. 37, no. 7, pp. 984–995, Jul. 1989. doi: 10.1109/29.32276.

[26] H. Krim and M. Viberg, "Two decades of array signal processing research: The parametric approach," *IEEE Signal Process. Mag.*, vol. 13, no. 4, pp. 67–94, Jul. 1996. doi: 10.1109/79.526899.

[27] X. Chen, Y. Morton, and F. Dovis, "A computationally efficient iterative MLE for GPS AOA estimation," *IEEE Trans. Aerosp. Electron. Syst.*, vol. 49, no. 4, pp. 2707–2716, Oct. 2013. doi: 10.1109/TAES.2013.6621847.

[28] M. T. Brenneman and Y. T. Morton, "A novel maximum likelihood estimator for GPS signal angle of arrival," in *Proc. Conf. Rec. 43rd Asilomar Conf. Signals, Syst. Comput.*, Pacific Grove, CA, USA, Nov. 2009, pp. 1154–1158. doi: 10.1109/ACSSC.2009.5470022.

[29] Z. Ping and H. Shi, "The integrated location algorithm based on fuzzy identification and data fusion with signal decomposition," in *Proc. Int. Conf. Fuzzy Syst. Knowl. Discovery*, 2005, pp. 383–387. doi: 10.1007/11539506_49.

[30] X. Tu, H. Zhang, X.-R. Cui, and T. A. Gulliver, "3-D TDOA/AOA location based on extended Kalman filter," in *Proc. 9th Int. Symp. Antennas, Propag. EM Theory*, Guangzhou, China, Nov./Dec. 2010, pp. 473–476. doi: 10.1109/ISAPE.2010.5696504.

[31] D. Kong and J. Chun, "A fast DOA tracking algorithm based on the extended Kalman filter," in *Proc. IEEE NAECON*, Dayton, OH, USA, Oct. 2000, pp. 235–238. doi: 10.1109/NAECON.2000.894916.

[32] J.-F. Gu, S. C. Chan, W.-P. Zhu, and M. N. S. Swamy, "Joint DOA estimation and source signal tracking with Kalman filtering and regularized QRD RLS algorithm," *IEEE Trans. Circuits Syst., II, Exp. Briefs*, vol. 60, no. 1, pp. 46–50, Jan. 2013. doi: 10.1109/TCSII.2012.2234874.

[33] A. Şen, C. Tansu, E. C. Ünlüsoy, M. Yurt, N. Evirgen, Ö. C. Sakinci, and B. Akbulut, "Proof of concept for satellite attitude determination using GNSS," in *Proc. RAST*, Istanbul, Turkey, Jun. 2015, pp. 163–168. doi: 10.1109/RAST.2015.7208334.

[34] V. Capuano, C. Botteron and P.-A. Farine, "GNSS based attitude determination systems for nanosatellites," in *Proc. 2nd IAA Conf. Dyn. Control Space Syst. (DYCOSS)*, Rome, Italy, Mar. 2014

[35] D. Niculescu and B. Nath, "Ad hoc positioning system (APS) using AOA," in *Proc. IEEE INFOCOM*, vol. 3, Mar./Apr. 2003, pp. 1734–1743. doi: 10.1109/INFCOM.2003.1209196.

[36] M. H. El-Shafey, T. Abdul-Rahman, and Y. H. Dakroury, "Relaxing the half-wavelength condition for estimating signal AoA at a line of sensors," in *Proc. 16th Eur. Signal Process. Conf.*, Lausanne, Switzerland, Aug. 2008, pp. 1–5.

[37] K. O'Keefe, M. Petovello, W. Cao, G. Lachapelle, and E. Guyader, "Comparing multicarrier ambiguity resolution methods for geometry-based GPS and galileo relative positioning and their application to low earth orbiting satellite attitude determination," *Int. J. Navigation Observ.*, vol. 2009, Art. no. 592073, Mar. 2009. doi: 10.1155/2009/592073.

[38] V. Syrjälä and M. Valkama, "Analysis and mitigation of phase noise and sampling jitter in OFDM radio receivers," *Int. J. Microw. Wireless Technol.*, vol. 2, no. 2, pp. 193–202, Apr. 2010. doi: 10.1017/S1759078710000309.

[39] D. Petrovic, W. Rave, and G. Fettweis, "Performance degradation of coded-OFDM due to phase noise," in *Proc. 57th IEEE Semiannu. Veh. Technol. Conf. (VTC)*, Jeju, South Korea, vol. 2, Apr. 2003, pp. 1168–1172. doi: 10.1109/VETECS.2003.1207811.

[40] *Jackson Labs GPSDO Oscillator*. Accessed: Jun. 28, 2019. [Online]. Available: http://www.jackson-labs.com/assets/uploads/main/LC_XO_specsheet.pdf

[41] *Octoclock*. Accessed: Dec. 5, 2018. [Online]. Available: https://www.ettus.com/product/details/OctoClock

[42] W. Lu, K. An, and T. Liang, "Robust beamforming design for sum secrecy rate maximization in multibeam satellite systems," *IEEE Trans. Aerosp. Electron. Syst.*, vol. 55, no. 3, pp. 1568–1572, Jun. 2019. doi: 10.1109/TAES.2019.2905306.

[43] K. An, M. Lin, T. Liang, J.-B. Wang, J. Wang, Y. Huang, and A. Lee Swindlehurst, "Performance analysis of multi-antenna hybrid satellite-terrestrial relay networks in the presence of interference," *IEEE Trans. Commun.*, vol. 63, no. 11, pp. 4390–4404, Nov. 2015. doi: 10.1109/TCOMM.2015.2474865.

[44] *ITU-R Ionospheric Propagation Recommendation*. Accessed: Jul. 14, 2019. [Online]. Available: https://www.itu.int/dms_pubrec/itu-r/rec/p/R-REC-P.531-11-201202-S!!PDF-E.pdf

[45] J. J. van de Beek, M. Sandell, and P. O. Borjesson, "ML estimation of time and frequency offset in OFDM systems," *IEEE Trans. Signal Process.*, vol. 45, no. 7, pp. 1800–1805, Jul. 1997. doi: 10.1109/78.599949.

[46] N. M. Balasubramanya, L. Lampe, G. Vos, and S. Bennett, "Low SNR uplink CFO estimation for energy efficient IoT using LTE," *IEEE Access*, vol. 4, pp. 3936–3950, 2016. doi: 10.1109/ACCESS.2016.2596679.

[47] T. Grelier, P.-Y. Guidotti, M. Delpech, J. Harr, J.-B. Thevenet, and X. Leyre, "Formation flying radio frequency instrument: First flight results from the PRISMA mission," in *Proc. NAVITEC*, Noordwijk, The Netherlands, Dec. 2010, pp. 1–8. doi: 10.1109/NAVITEC.2010.5708059.

[48] H. Minn and V. K. Bhargava, "An investigation into time-domain approach for OFDM channel estimation," *IEEE Trans. Broadcast.*, vol. 46, no. 4, pp. 240–248, Dec. 2000. doi: 10.1109/11.898744.

[49] M. Nassar, P. Schniter, and B. L. Evans, "A factor graph approach to joint OFDM channel estimation and decoding in impulsive noise environments," *IEEE Trans. Signal Process.*, vol. 62, no. 6, pp. 1576–1589, Mar. 2014. doi: 10.1109/TSP.2013.2295063.

[50] J.-B. Thevenet and T. Grelier, "Formation flying radio-frequency metrology validation and performance: The PRISMA case," *Acta Astron.*, vol. 82, no. 1, pp. 2–15, Jan. 2013. doi: 10.1016/j.actaastro.2012.07.034.

[51] *USRP 2952R*. Accessed: Dec. 5, 2018. [Online]. Available: http://www.ni.com/ro-ro/support/model.usrp-2952.html

[52] *LabVIEW Communications System Design Suite*. Accessed: Jul. 7, 2019. [Online]. Available: https://www.ni.com/ro-ro/shop/select/labview-communications-system-design-suite

[53] *ITU Radio Regulations*. Accessed: Jul. 3, 2019. [Online]. Available: http://search.itu.int/history/HistoryDigitalCollectionDocLibrary/1.43.48.en.101.pdf

[54] *AD-FMCOMMS5 MCS Board*. Accessed: Dec. 5, 2018. [Online]. Available: https://www.analog.com/en/design-center/evaluation-hardware-and-software/evaluation-boards-kits/eval-ad-fmcomms5-ebz.html

[55] L. Baroni and H. K. Kuga, "Analysis of attitude determination methods using GPS carrier phase measurements," *Math. Problems Eng.*, vol. 2012, Jan. 2012, Art. no. 596396. doi: 10.1155/2012/596396.

[56] G. Giorgi, P. J. G. Teunissen, S. Verhagen, and P. J. Buist, "Testing a new multivariate GNSS carrier phase attitude determination method for remote sensing platforms," *Adv. Space Res.*, vol. 46, no. 2, pp. 118–129, 2010. doi: 10.1016/j.asr.2010.02.023.

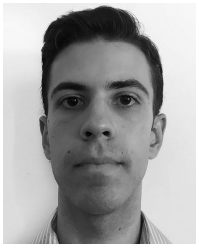

ALEXANDRU MIHAI CRISAN received the B.S. and M.S. degrees in electronics and telecommunications from the Faculty of Electronics, Telecommunications and Information Technology, University Politehnica of Bucharest (UPB), in 2013 and 2015, respectively. He is currently pursuing the Ph.D. degree with UPB. He is also a Research Engineer with the Research Center for Space Information CEOSpaceTech. His research interests include satellite constellations, wireless communications, and signal processing.

ALEXANDRU MARTIAN received the B.S. degree in electronics, the Ph.D. *(magna cum laude)* degree in telecommunications, and the Ph.D. degree in information technology from the University Politehnica of Bucharest, in 2000, 2013, and 2015, respectively. During his Ph.D. studies, he conducted several measurement campaigns for evaluating the spectrum occupancy in Romania and used USRP software defined radio platforms for implementing spectrum sensing applications for cognitive radio systems. From 2000 to 2007, he worked in telecommunication systems in Germany and Romania. Since 2007, he has been with the University Politehnica of Bucharest, where he is currently an Associate Professor with the Telecommunications Department, Faculty of Electronics, Telecommunications and Information Technology. He participated, as the Director or a Team Member, in several research projects, both national and international. He has published more than 40 papers in different scientific journals or in the proceedings of international conferences. His current research interests include wireless communication systems, with an emphasis on spectrum sensing based on energy detection, dynamic spectrum access, and cognitive radio. He regularly acts as a Reviewer of several journals, such as IEEE Access, the IEEE Communications Letters, *Future Generation Computer Systems*, and *Wireless Personal Communications*.

REMUS CACOVEANU received the M.S. degree in electronics and telecommunications from the University Politehnica of Bucharest (UPB), Romania, in 1983, and the Ph.D. degree in microwave, optics, and optoelectronics from the Institut National Polytechnique de Grenoble (INPG), France, in 1997. Since 1985, he has been a Professor of telecommunications with UPB. From 2000 to 2010, he was a System Architect with Redline Communications, Canada, and from 2011 to 2015, he was a Technical Consultant with Blinq Networks, Canada. His research interests include wireless communications systems, antennas, radar sensors, propagation, and microwave circuits.

DANIELA COLTUC was an Invited Professor with Universite Jean Monet in St Etienne, CPE Lyon, France, and a Researcher with the Laboratoire d'Automatique et Microinformatique Industrielle, Annecy, France, and Universite Lyon 2. In 2012, she joined the Research Center for Space Information CEOSpaceTech, Bucharest. She has a sound background in Information theory with applications in image processing. In the recent years, she has worked in computational imaging. She is currently a Full Professor with the University Politehnica of Bucharest, Romania.